Available online at www.sciencedirect.com

ScienceDirect

Advances in Space Research 72 (2023) 2051–2063

ADVANCES IN SPACE RESEARCH (a COSPAR publication)

www.elsevier.com/locate/asr

Regularized direct method for low–thrust trajectory optimization: Minimum–fuel transfer between cislunar periodic orbits

Kenta Oshima *

Hiroshima Institute of Technology, 2–1–1 Miyake, Hiroshima 731–5193, Japan

Received 28 January 2023; received in revised form 11 May 2023; accepted 30 May 2023
Available online 7 June 2023

Abstract

Low–thrust propulsion systems of high specific impulse are advantageous in the fuel efficiency. The fuel expenditure is further reduced together with optimization techniques though fuel–optimal low–thrust trajectories result in a discontinuous bang–bang control structure that can cause numerical difficulties. The present paper introduces regularized formulations into the direct multiple shooting method of minimizing fuel expenditure for low–thrust spacecraft trajectories. Instantaneous velocity changes approximating low–thrust maneuvers are expressed by regularized variables based on the Levi–Civita or Kustaanheimo–Stiefel transformation. The new formulation removes singularities due to null thrust impulses from derivatives of an objective function and constraints. The method automatically and robustly finds fuel–efficient bang–bang control structures for multi–revolutional transfers between periodic orbits in the Earth–Moon circular restricted three–body problem.

Keywords: Spacecraft trajectory optimization; Fuel minimization; Regularization; Direct multiple shooting; Low–thrust maneuver

1. Introduction

Minimizing fuel mass is one of the central problems for spacecraft trajectory design. Planetary or moon flyby (Vallado, 2013) and low–energy transport (Koon et al., 2011) are main techniques for reducing the fuel consumption from a dynamical point of view. Another aspect is the choice of a propulsion system. A conventional high–thrust chemical engine is able to produce a substantial velocity change (Δv) impulsively, though its relatively low specific impulse (I_{sp}) indicates the disadvantage in the fuel consumption. On the other hand, low–thrust propulsion such as an ion thruster takes longer time for producing the same amount of Δv, whereas the relatively high I_{sp} leads to higher fuel efficiency (Mazouffre, 2016).

Low–thrust propulsion requires complex processes for designing fuel–optimal trajectories. The determination of thrust arcs and the associated magnitude and direction of continuous maneuvers is a non–intuitive task. The Pontryagin's principle indicates a fuel–optimal solution possesses a discontinuous bang–bang control structure (Conway, 2010) that can cause numerical instability. A difficulty in finding good initial guess solutions arises from the many degrees of freedom of low–thrust maneuvers, but the convergence suffers from the quality of the initial guesses, especially for an indirect method that is based on the calculus of variations solving a sensitive boundary value problem (Russell, 2007). The homotopic approach has been used to improve the convergence property by solving a sequence of subproblems from an easier problem to a harder one having a small radius of convergence (Bertrand and Epenoy, 2002). The method has been able to compute fuel–optimal low–thrust solutions possessing the singular nature of the discontinuous bang–bang control

* Corresponding author.
E-mail address: k.oshima.nt@cc.it-hiroshima.ac.jp.

https://doi.org/10.1016/j.asr.2023.05.055
0273-1177/

profile (Jiang et al., 2012; Zhang et al., 2015; Pan et al., 2019). Recently, Taheri and Junkins (2018) proposed a smoothing technique using a hyperbolic tangent function to approximate the bang–bang control structure of fuel–optimal low–thrust solutions. Sidhoum and Oguri (2023) has indicated the superior performance of the hyperbolic tangent smoothing technique in terms of the computational efficiency and robustness within the indirect formulation of the fuel–optimal problem.

A direct method, on the other hand, solves a discretized nonlinear programming (NLP) problem by directly minimizing an objective function while satisfying constraints (Betts, 1998). The method is known to be less sensitive to initial guesses and easier for implementation. The Sims–Flanagan direct transcription method (Sims and Flanagan, 1999) has been one of the most commonly adopted procedures because of its simplicity and effectiveness. The method approximates low–thrust continuous maneuvers as a series of impulsive maneuvers in the multiple shooting framework. However, a solver cannot accurately update variables when one of the partial derivatives of an objective function or constraints with respect to variables faces a singularity. This is the case, when null control inputs exist, with equality constraints in terms of the mass continuity (Ellison et al., 2014). A mass–leak technique (Ottesen and Russell, 2021) has been known to avoid the singularities in an approximate manner by introducing a fictitious expression for the impulsive thrust magnitude. It is also possible to avoid the singularities by replacing small impulses with equality constraints enforcing the velocity continuity during the optimization (Oguri et al., 2020).

The present paper introduces regularizing techniques (Celletti, 2006) into a direct multiple shooting method to remove the singularities associated with the null control inputs. The regularizing techniques have been originally developed in the field of celestial mechanics for removing gravitational singularities at the center of a body through suitable changes of coordinates and time. The techniques even enable the computation of singular trajetories emanating from the gravitational center (Szebehely, 1967; Broucke, 1971; Oshima et al., 2017; Ollé et al., 2020). They are herein applied to remove the singularities in derivatives of an objective function and constraints in the field of optimal control.

In the remainder of the present paper, Section 2 highlights the singular nature of the non–regularized problem, summarizes the mass–leak technique, and introduces the novel regularized formulation. Planar (two–dimensional) and spatial (three–dimensional) formulations are developed based on the Levi–Civita and Kustaanheimo–Stiefel regularizations, respectively. Section 3 demonstrates the effectiveness of the regularized formulation by solving fuel–optimal low–thrust transfer problems from relatively simpler planar cases to more complicated spatial ones. The computational performance of the regularized method is compared with that in the non–regularized formulation adopting the mass–leak technique.

2. Problem formulation

I employ a multiple shooting procedure illustrated in Fig. 1, which divides a trajectory into segments via nodes, to reduce the sensitivity and improve the convergence. Note that the present paper adopts a multiple forward–shooting (Ottesen and Russell, 2021) variant for simplicity, whereas there are other works using a multiple forward– and backward–shooting procedure (Sims and Flanagan, 1999; Sims et al., 2006; Oguri et al., 2020) that can reduce the sensitivity in a greater manner. The use of the forward– and backward–shooting procedure may be suitable when facing a convergence issue.

In Fig. 1, a trajectory is divided into $N-1$ segments by N nodes with an equal time interval

$$\Delta t = \frac{t_N - t_1}{N-1} \tag{1}$$

leading to time at ith node

$$t_i = t_1 + (i-1)\Delta t, \tag{2}$$

and $\boldsymbol{r}_i, \boldsymbol{v}_i$, and $\boldsymbol{U}_i$ denote vectors of position, velocity, and regularized variables, respectively, at ith node.

On each node, an impulsive thrust vector

$$\Delta \boldsymbol{v}_i := \boldsymbol{v}_i^+ - \boldsymbol{v}_i^- \tag{3}$$

is defined corresponding to the discontinuity in the velocity vector. The empty and filled triangles as well as the superscripts of minus and plus indicate states before and after executing $\Delta \boldsymbol{v}_i$, respectively.

The change of the mass due to the execution of $\Delta \boldsymbol{v}_i$ is modeled according to the ideal rocket equation (Vallado, 2013)

$$m_i^+ = m_i^- e^{-\frac{|\Delta v_i|}{g_0 I_{sp}}}, \tag{4}$$

where $g_0 = 9.80665\ \mathrm{m/s^2}$ is the standard gravity, I_{sp} is the specific impulse of an engine, and a non–dimensional initial mass $m_1^- = 1$.

A series of small impulsive thrusts approximates continuous low–thrust maneuvers. Note that smaller Δt reduces the duration of a segment between discretized impulses and improves the accuracy of the approximation. The thrust magnitude during the segment between ith and $i+1$th nodes is approximated as (Ottesen and Russell, 2021)

$$T_i = m_i^+ \frac{|\Delta \boldsymbol{v}_i|}{\Delta t}. \tag{5}$$

The state after executing $\Delta \boldsymbol{v}_i$ $(i = 1, \ldots, N-1)$ are ballistically propagated from each node as

$$\begin{bmatrix} \boldsymbol{r}_{i+1}^- \\ \boldsymbol{v}_{i+1}^- \end{bmatrix} = \boldsymbol{\varphi}\left(\left\{\boldsymbol{r}_i^+, \boldsymbol{v}_i^+\right\}, t_i, t_{i+1}\right), \quad m_{i+1}^- = m_i^+, \tag{6}$$

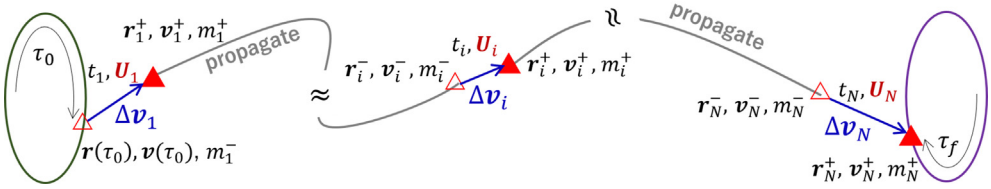

Fig. 1. A schematic figure illustrating a multiple forward–shooting procedure dividing a trajectory into $N-1$ segments by N nodes. At ith node, $\boldsymbol{r}_i$, $\boldsymbol{v}_i$, and $\boldsymbol{U}_i$ denote vectors of position, velocity, and regularized variables, respectively, and t_i and m_i represent time and mass, respectively. The empty and filled triangles as well as the superscripts of minus and plus indicate states before and after executing an impulsive maneuver Δv_i, respectively. τ_0 and τ_f parameterize departure and arrival points on initial and final orbits, respectively.

where $\boldsymbol{\varphi}\left(\left\{\boldsymbol{r}_i^+, \boldsymbol{v}_i^+\right\}, t_i, t_{i+1}\right)$ denotes the integration of the state $\left\{\boldsymbol{r}_i^+, \boldsymbol{v}_i^+\right\}$ from t_i to t_{i+1}. The dynamical system of interest in the present formulation is general and not limited to a specific model.

Time–like parameters τ_0 and τ_f describe the elapsed time for reaching the departure and arrival points from reference points on the initial and final orbits, respectively (Russell, 2007). States before the departure from the initial orbit and after the arrival to the final orbit are parametrized as $\{\boldsymbol{r}(\tau_0), \boldsymbol{v}(\tau_0)\}$ and $\left\{\boldsymbol{r}(\tau_f), \boldsymbol{v}(\tau_f)\right\}$, respectively. Note that reformulations of the current time–free, orbit–to–orbit transfer problem into simpler time–fixed or fixed–state transfer problems would be straightforward.

The first part of the remainder of this section is dedicated to highlight the singular nature of the non–regularized problem and summarize the mass–leak technique. The second part develops a regularized formulation based on the Levi–Civita and Kustaanheimo–Stiefel transformations to remove the singularities associated with null control inputs. The following subsections define NLP problems to be solved to compute fuel–optimal solutions.

2.1. Non–regularized formulation

In the non–regularized formulation, NLP variables usually include not only state vectors, but also the spacecraft mass (Sims et al., 2006). Let a set of NLP variables be

$$\boldsymbol{\xi} := \left\{\boldsymbol{r}_i^+, \boldsymbol{v}_i^+, m_i^+, t_1, t_N, \tau_0, \tau_f\right\}, \qquad i = 1, \ldots, N. \tag{7}$$

Since the fuel minimization problem aims to maximize the final spacecraft mass that is normalized by the initial mass, a natural choice of an objective function may be

$$J(\boldsymbol{\xi}) := -m_N^+, \tag{8}$$

analytic derivatives of which are straightforward to calculate owing to the inclusion of the mass in the NLP variables.

A solution must satisfy equality constraints

$$\boldsymbol{h}(\boldsymbol{\xi}) := \begin{bmatrix} \boldsymbol{\Psi}_1 \\ \boldsymbol{\Psi}_N \\ \boldsymbol{\Gamma}_i \\ M_i \end{bmatrix} = 0, \tag{9}$$

where

$$\boldsymbol{\Psi}_1 := \boldsymbol{r}_1^+ - \boldsymbol{r}(\tau_0), \tag{10}$$

$$\boldsymbol{\Psi}_N := \begin{bmatrix} \boldsymbol{r}_N^+ - \boldsymbol{r}(\tau_f) \\ \boldsymbol{v}_N^+ - \boldsymbol{v}(\tau_f) \end{bmatrix}, \tag{11}$$

$$\boldsymbol{\Gamma}_i := \boldsymbol{r}_i^+ - \boldsymbol{r}_i^-, \qquad i = 2, \ldots, N, \tag{12}$$

$$M_i := m_i^+ - m_i^- e^{-\frac{|\Delta v_i|}{g_0 I_{sp}}}, \qquad i = 1, \ldots, N, \tag{13}$$

and inequality constraints in accordance with Eq. (5)

$$\boldsymbol{g}(\boldsymbol{\xi}) := |\Delta v_i| - \frac{T_{max}}{m_i^+}\Delta t < \boldsymbol{0}, \qquad i = 1, \ldots, N, \tag{14}$$

where T_{max} is the maximum thrust magnitude available for the engine.

Since the equality constraints imposing the mass continuity in Eq. (13) depend on $\boldsymbol{v}_i^+$ through Eq. (3), the derivatives with respect to $\boldsymbol{v}_i^+$ include

$$\frac{\partial M_i}{\partial \boldsymbol{v}_i^+} = \frac{m_i^-}{g_0 I_{sp}} e^{-\frac{|\Delta v_i|}{g_0 I_{sp}}} \frac{\Delta v_i^{\mathrm{T}}}{|\Delta v_i|} \tag{15}$$

that is singular with the null control input $|\Delta v_i| = 0$ (Ellison et al., 2014).

Note that this singularity complicates the computation of fuel–optimal solutions that are known to exhibit the bang–bang control structure (Conway, 2010). During the optimization, unnecessary impulses included in an initial guess would be reduced down to zero magnitude facing the singularity and necessary impulses that are absence from the initial guess shall be generated from a coasting segment, where the singularity hinders the convergence.

2.1.1. Mass–leak technique

The mass–leak technique (Ottesen and Russell, 2021) introduces a constant ϵ ($|\epsilon| \ll 1$) and applies a fictitious expression for the impulsive thrust magnitude

$$|\Delta v_i^\epsilon| := \sqrt{|\Delta v_i|^2 + \epsilon^2} \tag{16}$$

to Eqs. (13) and (14) instead of the true magnitude $|\Delta v_i|$.

This scheme results in

$$\frac{\partial |\Delta v_i^\epsilon|}{\partial \boldsymbol{v}_i^+} = \frac{\Delta v_i^{\mathrm{T}}}{|\Delta v_i^\epsilon|} \tag{17}$$

and makes the derivative in Eq. (15) nonsingular as $|\Delta v_i^\epsilon|$ is always positive.

Of course, the scheme approximates the original problem and thus the true magnitude of velocity impulses, the corresponding mass in accordance with Eq. (4), and the thrust magnitude in Eq. (5) should be calculated from a post–converged solution (Ottesen and Russell, 2022). Smaller magnitude of ϵ improves the approximation at the cost of longer compuational time in general. Fig. 2 shows typical time histories of the magnitude of velocity impulses and the corresponding thrust magnitude in the cases of $\epsilon = 10^{-4}$ in the panels (a)–(c) and $\epsilon = 10^{-6}$ in the panels (d)–(f). It is clear that the case of $\epsilon = 10^{-6}$ better approximates the bang–bang control structure. However, the maximum values of the true thrust magnitude slightly deviate from $T_{max} = 0.04$ N due to the approximation and the solution in the case of $\epsilon = 10^{-6}$ is actually infeasible.

2.2. Regularized formulation

The central idea of a regularized formulation is to introduce a vector of regularized variables $\boldsymbol{U}_i$ such that

$$|\boldsymbol{\Delta v}_i| = |\boldsymbol{U}_i|^2, \qquad i = 1, \ldots, N, \tag{18}$$

into every node as illustrated in Fig. 1. This expression, together with the addition of the regularized variables to the NLP variables, is effective in removing the singularities as the derivative

$$\frac{\partial |\boldsymbol{\Delta v}_i|}{\partial \boldsymbol{U}_i} = 2\boldsymbol{U}_i^{\mathrm{T}} \tag{19}$$

is nonsingular without any approximations.

Since the spacecraft mass, which depends on $|\boldsymbol{\Delta v}_i|$ through Eq. (4), is herein directly representable via $\boldsymbol{U}_i$ through Eq. (18) as

$$m_i^+ = e^{-\frac{\sum_{k=1}^{i} |U_k|^2}{g_0 I_{sp}}}, \qquad i = 1, \ldots, N, \tag{20}$$

m_i^+ is no longer included in NLP variables. Thus, let a set of NLP variables in the regularized formulation be

$$\boldsymbol{\xi} := \left\{ \boldsymbol{r}_i^+, \boldsymbol{v}_i^+, \boldsymbol{U}_i, t_1, t_N, \tau_0, \tau_f \right\}, \qquad i = 1, \ldots, N. \tag{21}$$

2.2.1. Planar case

In a two–dimensional planar problem, I introduce components of the vector of regularized variables at each node

$$\boldsymbol{U}_i := \begin{bmatrix} u_i \\ w_i \end{bmatrix} \tag{22}$$

and express x– and y–components of the impulsive thrust vector by adopting the Levi–Civita transformation (Celletti, 2006)

$$\boldsymbol{\Delta v}_i := \begin{bmatrix} \Delta v_{xi} \\ \Delta v_{yi} \end{bmatrix} = \begin{bmatrix} u_i^2 - w_i^2 \\ 2u_i w_i \end{bmatrix}, \tag{23}$$

which satisfy Eq. (18).

According to Eqs. (8) and (20), a natural choice of an objective function may be

$$J(\boldsymbol{\xi}) := \sum_{i=1}^{N} \left(u_i^2 + w_i^2 \right) = \sum_{i=1}^{N} |\boldsymbol{U}_i|^2, \tag{24}$$

derivatives of which are nonsingular owing to the inclusion of the regularized variables in the NLP variables.

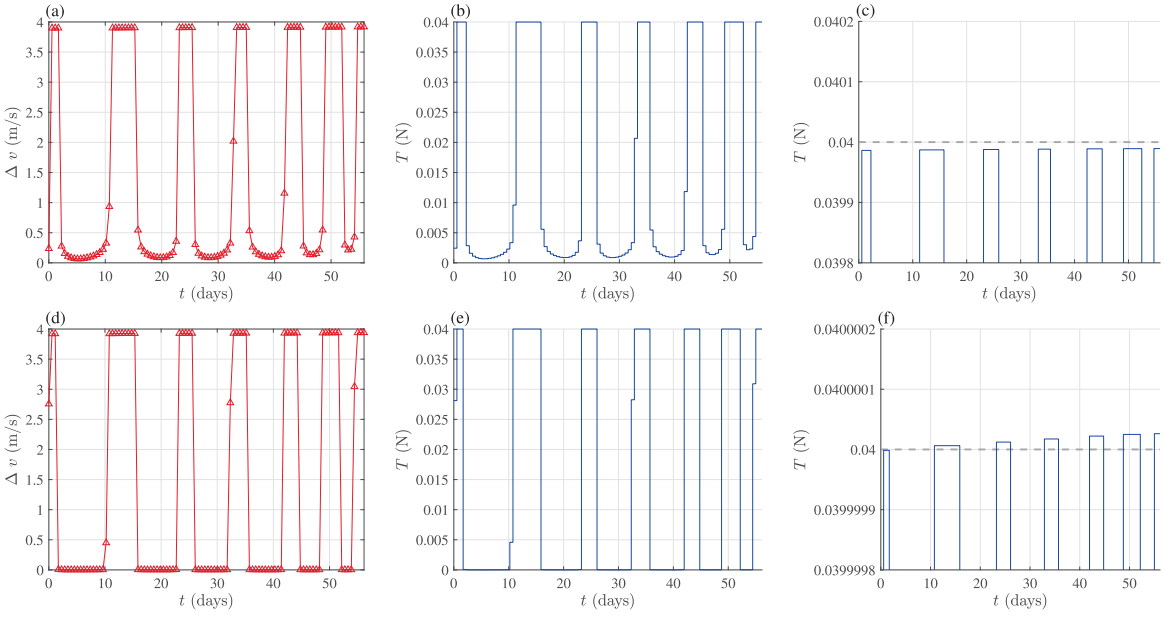

Fig. 2. Typical time histories of the magnitude of velocity impulses and the corresponding thrust magnitude and its amplification around $T_{max} = 0.04$ N in the cases of $\epsilon = 10^{-4}$ (panels (a)–(c)) and $\epsilon = 10^{-6}$ (panels (d)–(f)).

Since the spacecraft mass at each node is directly computable from Eq. (20), the equality constraints in Eq. (13) imposing the mass continuity are no longer necessary. I thus set the following equality constraints in the regularized formulation

$$\boldsymbol{h}(\boldsymbol{\xi}) := [\,\boldsymbol{\Psi}_1\ \boldsymbol{\Psi}_N\ \boldsymbol{\Gamma}_i\ \boldsymbol{\Omega}_i\,]^{\mathrm{T}} = 0, \tag{25}$$

where $\boldsymbol{\Psi}_1, \boldsymbol{\Psi}_N$, and $\boldsymbol{\Gamma}_i$ are identical to Eqs. (10)–(12), respectively, and the constraints peculiar to the regularized formulation

$$\boldsymbol{\Omega}_i := \boldsymbol{v}_i^+ - \boldsymbol{v}_i^- - \begin{bmatrix} u_i^2 - w_i^2 \\ 2u_i w_i \end{bmatrix} = 0, \qquad \boldsymbol{v}_1^- := \boldsymbol{v}(\tau_0), \qquad i = 1, \ldots, N, \tag{26}$$

bring the physical meaning into the regularized variables in the NLP problem naturally arising from the expression in Eq. (23).

Substituting Eqs. (18) and (20) into Eq. (14) yields inequality constraints

$$\boldsymbol{g}(\boldsymbol{\xi}) := |\boldsymbol{U}_i|^2 - e^{\frac{\sum_{k=1}^{i}|\boldsymbol{U}_k|^2}{g_0 I_{sp}}} T_{max}\Delta t < \boldsymbol{0}, \qquad i = 1, \ldots, N, \tag{27}$$

the derivatives of which are nonsingular.

An inverse transformation of Eq. (23) is necessary when initializing the regularized variables from impulsive thrust vectors of a certain initial guess solution. Table 1 summarizes the inverse transformation for the initialization of the regularized variables.

2.2.2. Spatial case

In a three–dimensional spatial problem, the regularized variables

$$\boldsymbol{U}_i := \begin{bmatrix} u_i \\ w_i \\ s_i \end{bmatrix} \tag{28}$$

are introduced to express the impulsive velocity vector based on the Kustaanheimo–Stiefel transformation (Celletti, 2006)

$$\Delta\boldsymbol{v}_i := \begin{bmatrix} \Delta v_{xi} \\ \Delta v_{yi} \\ \Delta v_{zi} \end{bmatrix} = \begin{bmatrix} u_i^2 - w_i^2 - s_i^2 \\ 2u_i w_i \\ 2u_i s_i \end{bmatrix}, \tag{29}$$

which also satisfy Eq. (18).

Similarly to the planar formulation, I define an objective function

$$J(\boldsymbol{\xi}) := \sum_{i=1}^{N}\left(u_i^2 + w_i^2 + s_i^2\right) = \sum_{i=1}^{N}|\boldsymbol{U}_i|^2, \tag{30}$$

and constraints, the expressions of which are identical to Eqs. (25) and (27), respectively. An exception arises from Eq. (29) such that the equality constraints peculiar to the three–dimensional regularized formulation become

$$\boldsymbol{\Omega}_i := \boldsymbol{v}_i^+ - \boldsymbol{v}_i^- - \begin{bmatrix} u_i^2 - w_i^2 - s_i^2 \\ 2u_i w_i \\ 2u_i s_i \end{bmatrix} = \boldsymbol{0}, \qquad i = 1, \ldots, N. \tag{31}$$

An inverse transformation of Eq. (29) summarized in Table 2 is more complicated than that in the planar case. Indeed, w_i and s_i are indefenite in the third condition.

One possible solution is to give special treatment to the node satisfying the third condition. I rearrange the expression in Eq. (29) and the corresponding part of the equality constraints in Eq. (31) specifically for the node as

$$\Delta\boldsymbol{v}_i := \begin{bmatrix} \Delta v_{xi} \\ \Delta v_{yi} \\ \Delta v_{zi} \end{bmatrix} = \begin{bmatrix} 2u_i w_i \\ u_i^2 - w_i^2 - s_i^2 \\ 2u_i s_i \end{bmatrix}, \tag{32}$$

$$\boldsymbol{v}_i^+ - \boldsymbol{v}_i^- - \begin{bmatrix} 2u_i w_i \\ u_i^2 - w_i^2 - s_i^2 \\ 2u_i s_i \end{bmatrix} = \boldsymbol{0}. \tag{33}$$

Note that the objective function in Eq. (30) and its derivatives are invariant under this rearrangement. Table 3 summarizes an inverse transformation of Eq. (32) that can be used to initialize regularized variables on the nodes satisfying the condition.

3. Demonstration

This section presents some examples of applying the regularized formulation to trajectory optimization problems and compares the performance with that in the non–regularized formulation adopting the mass–leak technique.

Table 1
An inverse transformation of Eq. (23).

Condition	u_i	w_i
$\Delta v_{xi} > 0$	$\sqrt{\frac{\lvert\Delta\boldsymbol{v}_i\rvert+\Delta v_{xi}}{2}}$	$\frac{\Delta v_{yi}}{2u_i}$
$\Delta v_{xi} < 0$	$\frac{\Delta v_{yi}}{2w_i}$	$\sqrt{\frac{\lvert\Delta\boldsymbol{v}_i\rvert-\Delta v_{xi}}{2}}$
$\Delta v_{xi} = 0$ & $\Delta v_{yi} \geqslant 0$	$\sqrt{\frac{\Delta v_{yi}}{2}}$	$\sqrt{\frac{\Delta v_{yi}}{2}}$
$\Delta v_{xi} = 0$ & $\Delta v_{yi} < 0$	$\sqrt{\frac{-\Delta v_{yi}}{2}}$	$-\sqrt{\frac{-\Delta v_{yi}}{2}}$

Table 2
An inverse transformation of Eq. (29).

Condition	u_i	w_i	s_i
$\Delta v_{xi} > 0$	$\sqrt{\frac{\lvert\Delta\boldsymbol{v}_i\rvert+\Delta v_{xi}}{2}}$	$\frac{\Delta v_{yi}}{2u_i}$	$\frac{\Delta v_{zi}}{2u_i}$
$\Delta v_{xi} \leqslant 0$ & $\Delta v_{yi}^2 + \Delta v_{zi}^2 > 0$	$\sqrt{\frac{\lvert\Delta\boldsymbol{v}_i\rvert+\Delta v_{xi}}{2}}$	$\frac{\Delta v_{yi}}{2u_i}$	$\frac{\Delta v_{zi}}{2u_i}$
$\Delta v_{xi} < 0$ & $\Delta v_{yi} = \Delta v_{zi} = 0$	0	–	–
$\lvert\Delta\boldsymbol{v}_i\rvert = 0$	0	0	0

Table 3
An inverse transformation of Eq. (32).

Condition	u_i	w_i	s_i
$\Delta v_{xi} < 0$ & $\Delta v_{yi} = \Delta v_{zi} = 0$	$\sqrt{\frac{-\Delta v_{xi}}{2}}$	$-\sqrt{\frac{-\Delta v_{xi}}{2}}$	0

3.1. Mathematical model

Although the formulations in the previous section are model–free, I adopt the circular restricted three–body problem (Szebehely, 1967) in the following examples to model spacecraft trajectories in the Earth–Moon system as it is simple and accurate enough for capturing the main dynamics. The model describes the motion of a massless particle (spacecraft) moving under gravitational effects of two celestial bodies (Earth and Moon) rotating around their barycenter in circular orbits.

A rotating frame that corotates with the celestial bodies is useful for expressing equations of motion in a time–independent autonomous form

$$\dot{v}_x = 2v_y - \frac{\partial \overline{U}}{\partial x}, \quad \dot{v}_y = -2v_x - \frac{\partial \overline{U}}{\partial y}, \quad \dot{v}_z = -\frac{\partial \overline{U}}{\partial z}, \tag{34}$$

where

$$\overline{U} := -\frac{1}{2}\left(x^2 + y^2\right) - \frac{1-\mu}{r_1} - \frac{\mu}{r_2} - \frac{1}{2}\mu(1-\mu), \tag{35}$$

$$r_1 := \sqrt{(x+\mu)^2 + y^2 + z^2}, \tag{36}$$

$$r_2 := \sqrt{(x-1+\mu)^2 + y^2 + z^2}, \tag{37}$$

and μ is a constant representing the mass ratio between the Earth and the Moon. Table 4 summarizes physical constants in the Earth–Moon system used in the present paper.

A planar problem considers an initial condition $z = v_z = 0$, which restricts the motion of a particle to the xy–plane according to Eq. (34). Otherwise, the particle can exhibit the out–of–plane motion in the three–dimensional space that is termed a spatial problem.

The system possesses an integral of motion called the Jacobi constant

$$C := -\left(v_x{}^2 + v_y^2 + v_z^2\right) - 2\overline{U}, \tag{38}$$

which is the only integral of motion. The Jacobi constant indicates an energy level such that its higher value corresponds to a less energetic motion of a particle.

The model admits the existence of five equilibrium points and periodic orbits that are central in theoretical analyses and are useful in applications (Koon et al., 2011). Fig. 3 shows periodic orbits used in the demonstrations below. The distant retrograde orbits (DROs) are planar orbits that are linearly stable (Hénon, 1969; Lam and Whiffen, 2005). The planar and vertical Lyapunov orbits (pL and vL) are unstable orbits associated with one of the equilibria L_1 with $C = 3.04$. It is noteworthy that the planar Lyapunov orbit at the energy level possesses not only the horizontal in–plane instability but also the vertical out–of–plane instability (Hénon, 1974), with which stable and unstable manifolds playing the role of natural transport pathways between in–plane and out–of–plane orbits associate (Oshima, 2019; Oshima, 2021). Table 5 summarizes the state at a reference point defined by the time–like parameter $\tau = 0$ (see Section 2) and the period of the four periodic orbits.

Table 4
Physical constants in the Earth–Moon system (Topputo, 2013).

Name	Value	Unit
Distance unit	3.84405000×10^8	m
Time unit	4.34811305	day
Velocity unit	1.02323281×10^3	m/s
Mass parameter μ	0.0121506683	–

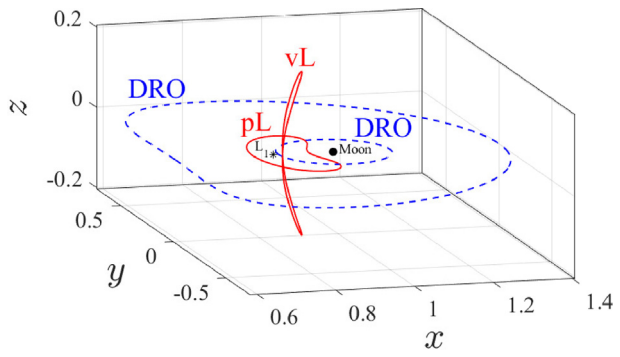

Fig. 3. Distant retrograde orbits (DROs) and planar and vertical Lyapunov orbits (pL and vL) associated with an equilibrium point L_1 shown in the Earth–Moon rotating frame.

3.2. Implementation

I solve the NLP problems by using the MATLAB's nonlinear constrained optimization solver fmincon. The sequential quadratic programming algorithm (Gill et al., 1981) is adopted with termination tolerances of 10^{-10} on the violation of the constraints, the first–order optimality, and the step size. Analytic derivatives of the objective function and the constraints are provided. Trajectories are integrated by a variable–step Runge–Kutta–Fehlberg algorithm of orders 7 and 8 with a tolerance of 10^{-13}. All simulations use a Windows 11 laptop with an Intel i7–1185G7 CPU and a 3.00 GHz clock speed.

When implementing the mass–leak technique in the non–regularized formulation for comparison, the value of ϵ must be specified. I investigate the cases of $\epsilon = 10^{-4}$ and 10^{-6} that are considered to be practical (Ottesen and Russell, 2021). Additionally, the spacecraft mass m_i^+ $(i = 1, \ldots, N)$ is initialized by using Eq. (4) based on the magnitude of the discontinuity in the velocity vector on each node of an initial guess solution. This exhibits slightly better convergences than uniformly initializing $m_i^+ = 1$.

Since the circular restricted three–body problem used in the demonstrations next is a time–independent autono-

Table 5
Non–dimensional state (x, y, z, v_x, v_y, v_z) and period T of the four periodic orbits in Fig. 3.

Name	x	y	z	v_x	v_y	v_z	T
Larger DRO	0.586792825	0	0	0	0.956849854	0	5.68936129
Smaller DRO	0.849470547	0	0	0	0.479391525	0	2.30841488
Planar Lyapunov	0.784707463	0	0	0	0.432153743	0	3.84947313
Vertical Lyapunov	0.908282483	0	0.204570695	0	−0.0552436507	0	3.70274690

mous system, I fix $t_1 = 0$ and remove it from the NLP variables. Thus, t_N represents the flight time. Incorporating t_1 into the NLP variables, which is beyond the present demonstrations, would be able to handle optimization problems in higher–fidelity dynamical systems explicitly depend on time.

I assume a spacecraft of 500 [kg] initial mass equipped with a low–thrust engine of $I_{sp} = 3000$ [s] and $T_{max} = 0.04$ [N] that closely follow the parameters in JAXA's DESTINY$^+$ (Ozaki et al., 2022).

3.3. Planar case

This example considers planar low–thrust transfer from the larger DRO to the smaller DRO in Fig. 3. Note that constructing an initial guess solution for fuel–optimal transfer between stable periodic orbits is not straightforward due to the absence of stable or unstable manifolds that are often used for computing fuel–efficient trajectories (Koon et al., 2011; Mingotti et al., 2011). Therefore, the present study generates an initial guess solution by simply

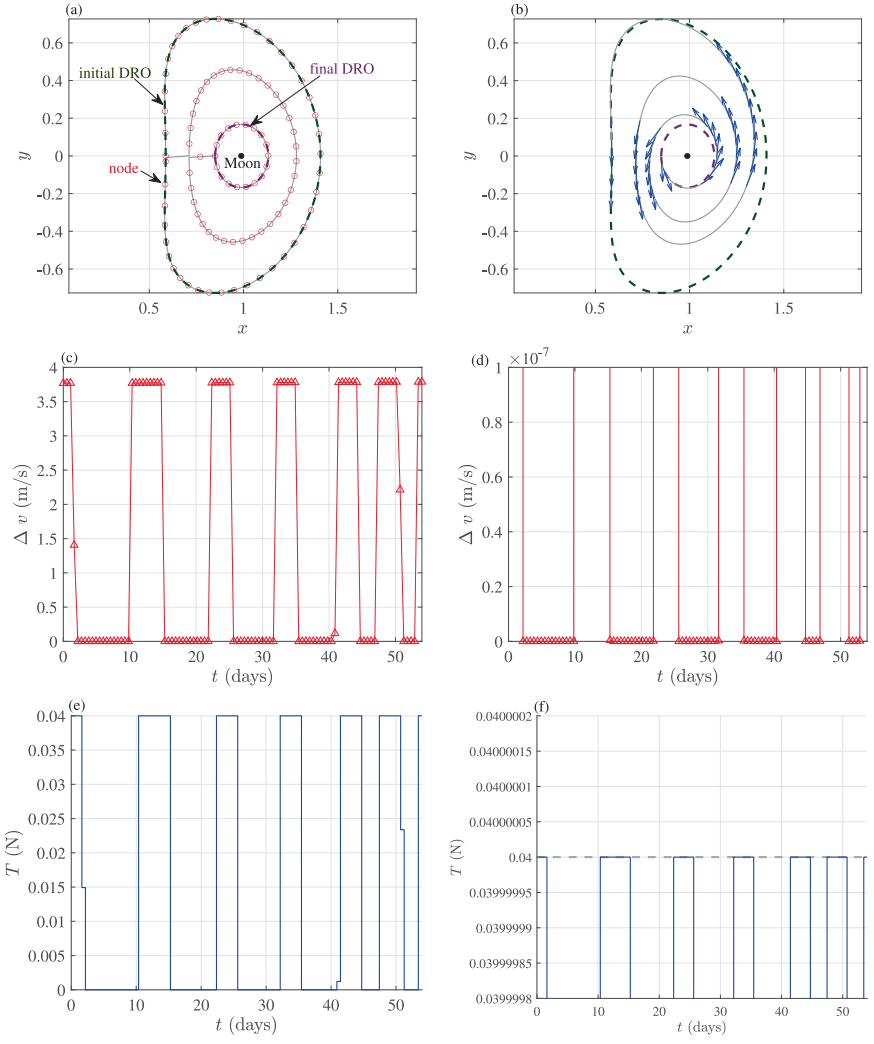

Fig. 4. Low–thrust transfer from the larger DRO (green broken curve) to the smaller DRO (purple broken curve). (a) An initial guess trajectory (gray) composed of three DROs with 100 nodes (red circle). (b) An optimal trajectory (gray) with thrust vectors (blue arrow). (c) Time history of the magnitude of velocity impulses and (d) the amplification. (e) Time history of the thrust magnitude and (f) the amplification.

patching multiple DROs with an equal interval of the Jacobi constant from the initial to final ones with $\tau_0 = \tau_f = 0$.

Fig. 4(a) shows an initial guess composed of three DROs and 100 nodes in total. Note that substantial gaps exist between the DROs. Fig. 4(b)–(f) exhibit a fuel–optimal solution computed by the regularized method. The panel (b) presents an optimal transfer trajectory with thrust vectors. The number of DROs in the initial guess and the number of revolutions in the converged solution are consistent. The panels (c) and (d) show the time history of velocity impulses and its amplification, respectively, indicating the reduction of the unnecessary impulses below 10^{-8} m/s that is less than 10^{-11} in non–dimensional units owing to the removal of the singularities in the regularized formulation. It is also noteworthy that many of the thrust impulses appear from the initially ballistic arcs again due to the non–singular nature of the present method. The panel (e) indicates the bang–bang structure of the thrust magnitude that is computed from Eq. (5). Since the trajectory is divided with an equal Δt, the bang–bang structure is imperfect in appearance corresponding to the intermediate Δv magnitude at $t \approx 2, 41, 51$ days in the panel (c). However, the solution indeed possesses a perfect bang–bang structure as one can fictitiously move a node belonging to a coasting segment just before or after the imperfect thrust structure to shorten Δt without affecting the solution so that the corresponding thrust magnitude reaches its maximum level. The panel does not cover the thrust segment associated with the final impulse in accordance with the definition of Eq. (5). The panel (f) shows the amplification of the panel (e) around $T_{max} = 0.04$ N indicating more accurate generations of the maximum thrust magnitude than those of the mass–leak technique in the non–regularized formulation, the corresponding results of which are shown in Fig. 2. The optimal solution results in $m_N^+ = 497.502$ kg, the total $\Delta v = 147.326$ m/s, and $t_N = 53.984$ days.

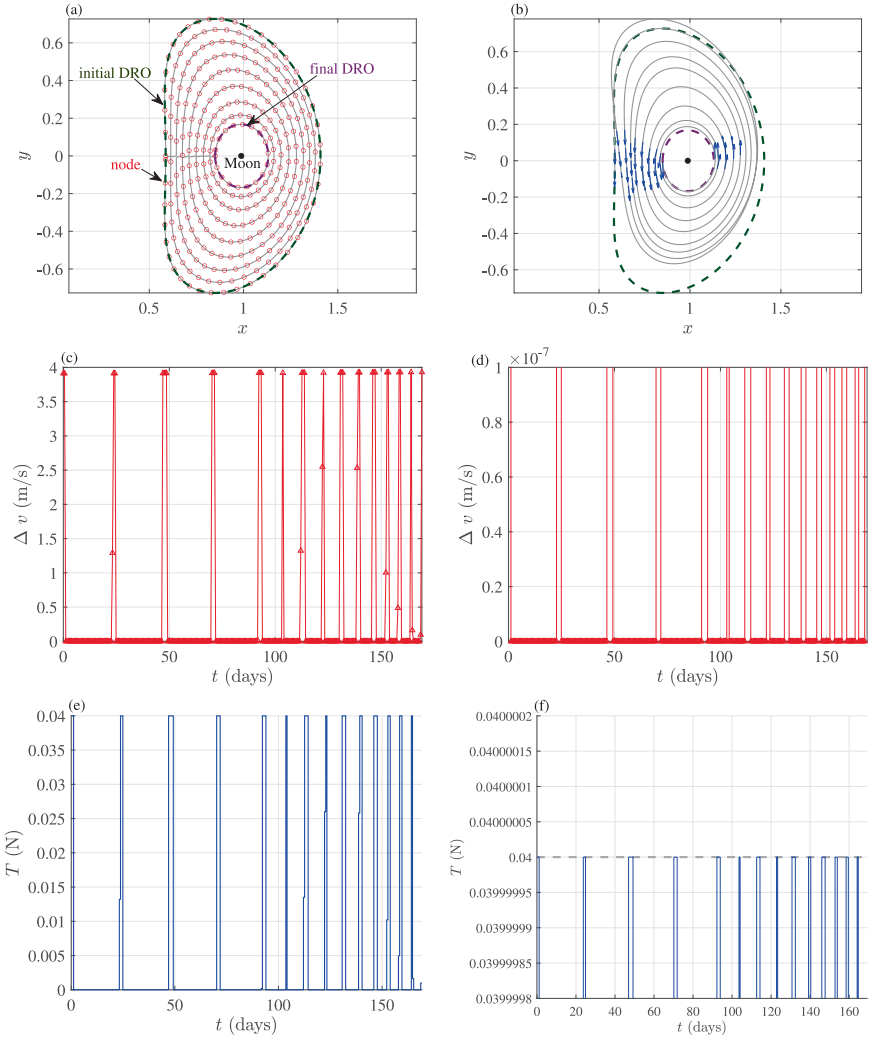

Fig. 5. Low–thrust transfer from the larger DRO (green broken curve) to the smaller DRO (purple broken curve). (a) An initial guess trajectory (gray) composed of nine DROs with 300 nodes (red circle). (b) An optimal trajectory (gray) with thrust vectors (blue arrow). (c) Time history of the magnitude of velocity impulses and (d) the amplification. (e) Time history of the thrust magnitude and (f) the amplification.

The regularized method is further tested in a more complicated scenario that performs more revolutions between the same DROs. Fig. 5 presents an initial guess composed of nine DROs and an optimal solution using 300 nodes. It still converges to a satisfactory solution exhibiting the accurate bang–bang control structure with smaller fuel consumption and longer time–of–flight than the previous case. The additional revolutions lead to the disappearance of the thrust arcs near apogees and the asymmetric geometry in the initial part of the transfer. The optimal solution results in $m_N^+ = 497.646$ kg, the total $\Delta v = 138.850$ m/s, and $t_N = 169.197$ days.

3.4. Spatial case

This example considers low–thrust transfer from the vertical Lyapunov orbit to the planar Lyapunov orbit in Fig. 3 requiring a substantial inclination change in the three–dimensional space. Since both of the initial and final orbits are unstable possessing stable and unstable manifolds (Koon et al., 2011) that are asymptotic to them, I add an inequality constraint in terms of the flight time $t_N < 90$ days to avoid searching for a solution of infinitely long time–of–flight with an infinitesimally small departure or arrival maneuver (Bokelmann and Russell, 2020).

Fig. 6(a) shows an initial guess solution divided by 200 nodes. The impulsive transfer solution "vL–(i)" leveraging the vertical out–of–plane instability associated with the planar Lyapunov orbit obtained in the author's previous work (Oshima, 2021) is adopted for an initial guess. The solution includes departure and arrival maneuvers of approximately 55 m/s and 20 m/s, respectively, which is far from a low–thrust trajectory. The other panels exhibit a fuel–optimal solution computed by the regularized method. The panel (b) presents an optimal transfer trajectory with thrust vectors, which are intuitively consistent for efficiently changing the orbital plane. Note that most of the plane changes are ballistically achieved via the out–of–plane instability. The panels (c) and (d) show the time history of impulses and its amplification, respectively, demonstrating again the ability of reducing unnecessary impulses and generating necessary impulses. It is interesting that the large departure maneuver in the initial guess solution is reduced to the isolated, small impulse leading to a fuel–ef-

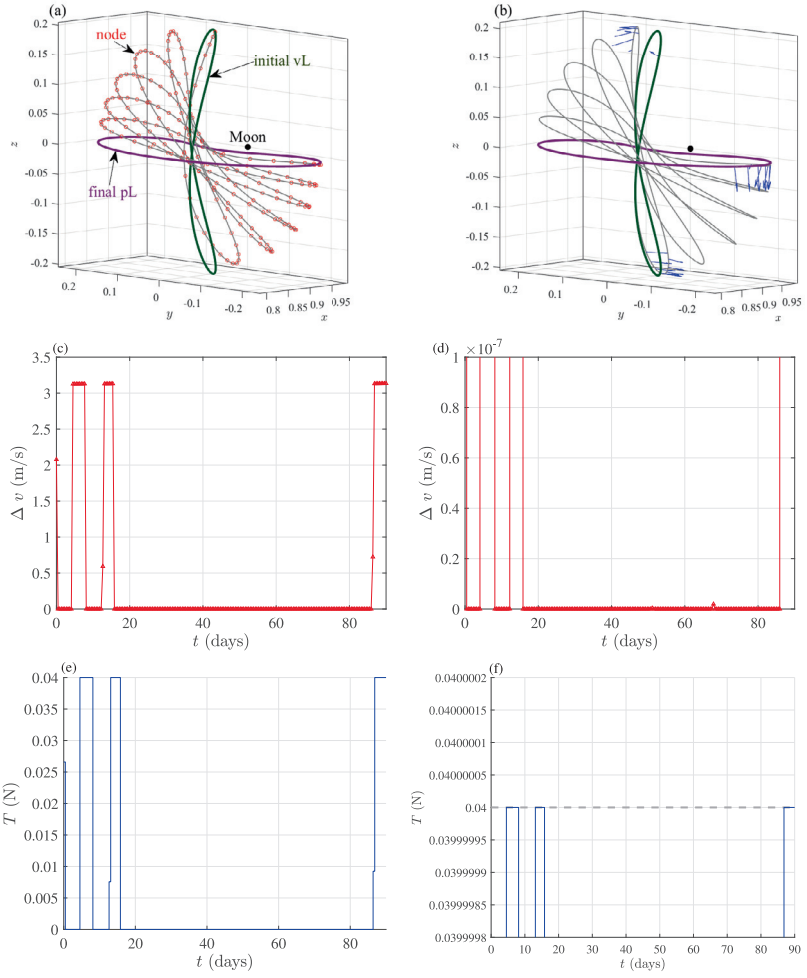

Fig. 6. Low–thrust transfer from the vertical Lyapunov orbit (vL, green curve) to the planar Lyapunov orbit (pL, purple curve). (a) An initial guess trajectory (gray) divided by 200 nodes (red circle). (b) An optimal trajectory (gray) with thrust vectors (blue arrow). (c) Time history of the magnitude of velocity impulses and (d) the amplification. (e) Time history of the thrust magnitude and (f) the amplification.

ficient, unstable manifold–like departure from the vertical Lyapunov orbit. The panels (e) and (f) show the time history of the thrust magnitude and its amplification, respectively, that are characterized by the bang–bang control structure. The optimal solution results in $m_N^+ = 498.773$ kg, the total $\Delta v = 72.257$ m/s, and $t_N = 90.000$ days.

In comparison with a similar fuel–optimal low–thrust transfer between planar and vertical Lyapunov orbits associated with L_2 in the Earth–Moon system (Pritchett et al., 2018), the present solution achieves approximately 75% reduction of the total Δv with even a shorter flight time. The reason for this substantial difference seems to arise from the different ways of generating initial guess solutions: Pritchett et al. (2018) patched axial orbits (Doedel et al., 2003) as the family naturally connects the planar and vertical Lyapunov families whereas Oshima (2021) used a stable manifold associated with the vertical instability of the planar Lyapunov family as it ballistically connects planar and spatial orbits. Indeed, the energy levels of the axial family and the vertical instability of the planar Lyapunov family do not overlap. Thus, an initial guess solution composed of the axial orbits requires plane change maneuvers whereas one leveraging the vertical instability needs maneuvers for transferring into a state that is able to ballistically change its inclination. The above comparison indicates that the latter results in much smaller fuel expenditure. I conjecture that the use of the vertical instability may also reduce the fuel cost in a similar application considering low–thrust transfer between planar and vertical Lyapunov orbits through the axial family (Sullivan et al., 2021).

Although a greater number of nodes improves the accuracy of the discrete approximation of low–thrust continuous maneuvers as noted, it may also be interesting to roughly assess a fuel–optimal solution with a less number of nodes and a lower computational burden. Fig. 7 presents an initial guess and optimized results for the same problem as the previous one using a half number of nodes, i.e., $N = 100$. The maximum magnitude of the velocity impulses is almost double in accordance with Eqs. (1) and (27). The converged solution matches the previous one quite well except for the tiny impulse at $t \approx 82$ days,

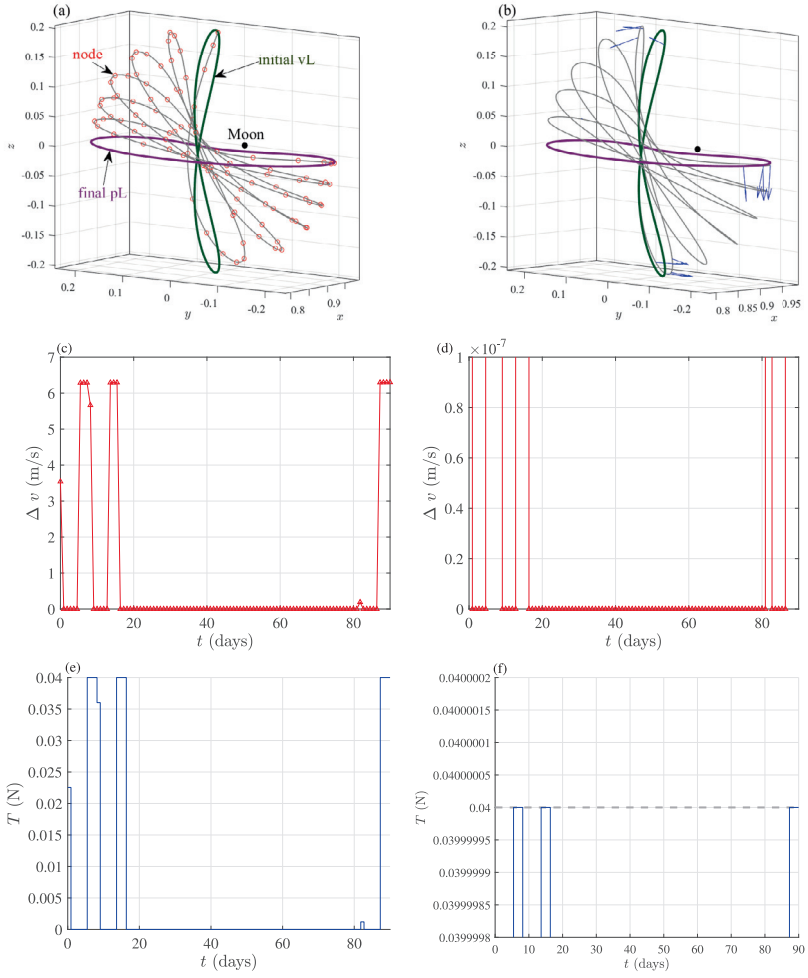

Fig. 7. Low–thrust transfer from the vertical Lyapunov orbit (vL, green curve) to the planar Lyapunov orbit (pL, purple curve). (a) An initial guess trajectory (gray) divided by 100 nodes (red circle). (b) An optimal trajectory (gray) with thrust vectors (blue arrow). (c) Time history of the magnitude of velocity impulses and (d) the amplification. (e) Time history of the thrust magnitude and (f) the amplification.

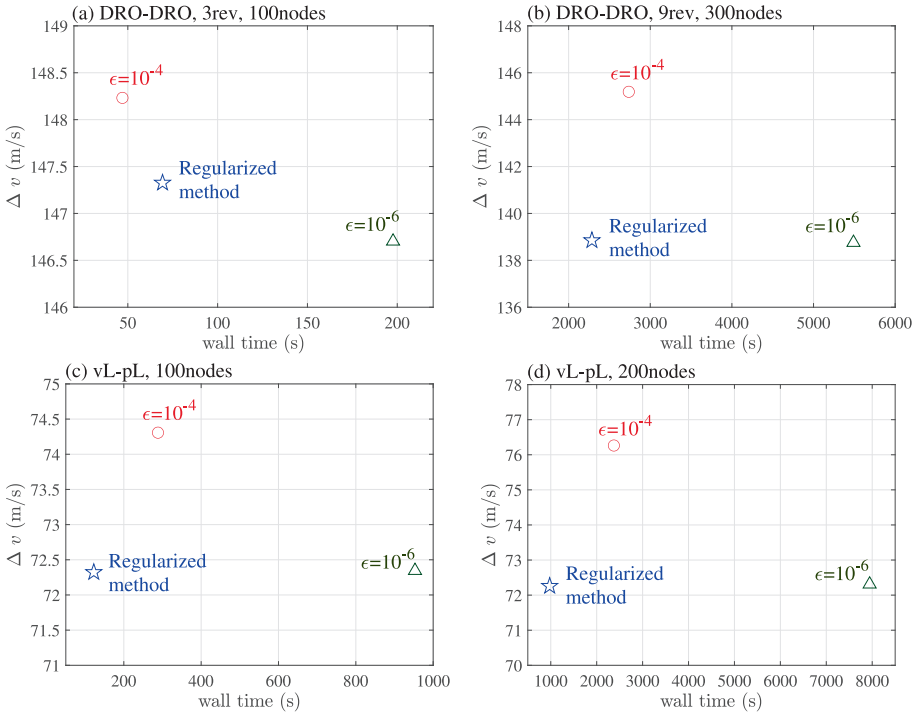

Fig. 8. Performance of the regularized method (star) and the mass–leak technique (circle for $\epsilon = 10^{-4}$ and triangle for $\epsilon = 10^{-6}$) in terms of the wall–clock time until the convergence and the total Δv of the converged solutions. Top of each panel indicates the corresponding problem.

the necessity of which for the optimality cannot be explained. Since the impulse disappears with a greater number of nodes, the solution seems to be suboptimal, but accurate enough for a rough estimate for this problem. The converged solution results in $m_N^+ = 498.772$ kg, the total $\Delta v = 72.322$ m/s, and $t_N = 90.000$ days. The suboptimality leads to the slightly smaller final mass and larger total Δv than those in the previous example.

3.5. Comparative performance

This section compares the performance of the regularized method and the mass–leak technique in the non–regularized formulation for solving the four examples above. Both of the methods successfully converge in all of the cases.

Fig. 8 exhibits the comparison in terms of the wall–clock time until the convergence and the total Δv of the converged solutions. The panels (a), (b), (c), and (d) correspond to the examples in Figs. 4, 5, 7, and 6, respectively, as indicated on the top of each of them.

In the simplest example of the 3–revolutional planar DRO–DRO transfer, the performance of the regularized method is at a glance in between those of $\epsilon = 10^{-4}$ and 10^{-6} in the mass–leak technique as shown in the panel (a). The inferiority in the case of $\epsilon = 10^{-4}$ in terms of the total Δv would be caused by the non–optimal small impulses in Fig. 2(a) that should be null impulses for the optimal solution. Although tiny non–optimal impulses exist in the case of $\epsilon = 10^{-6}$ as well, the infeasible thrust magnitude in Fig. 2(f) may cause its apparent superiority in terms of the total Δv. When tolerating the inaccuracy with respect to Δv, the case of $\epsilon = 10^{-4}$ seems to be superior considering the fast convergence.

The more complicated examples possessing more revolutions or another degree of freedom indicate the favorable performance of the regularized method as shown in Fig. 8 (b)–(d). Its superiority in terms of the total Δv could be due to the greater portion of the coasting duration with respect to the total flight time in these examples, which increases the cumulative effect of the non–optimal impulses in the mass-leak technique and limits the influence of the infeasible thrust magnitude. The regularized method also exhibits the superiority in terms of the computational time in these examples achieving 17% to 88% reduction.

Note that the regularized method saves the effort of tuning ϵ, the appropriate value of which can differ for each purpose. In summary, the results and the comparisons above demonstrate another promising option to solve complex low–thrust trajectory optimization problems.

4. Conclusion

The present paper formulated NLP problems to be solved to compute fuel–optimal low–thrust spacecraft trajectories by removing notorious singularities associated with null velocity impulses. The introduction of the novel NLP variables expressing velocity impulses based on the Levi–Civita or Kustaanheimo–Stiefel transformation regularized the problem. The removal of the singularities

enabled automatic and robust convergence into fuel–efficient solutions exhibiting the bang–bang control structure from initial guess solutions possessing substantial position discontinuities or large impulses. The method was applied to optimize multi–revolutional transfers between periodic orbits including a sensitive, unstable manifold–guided solution synergestically leveraging dynamical and propulsive characteristics to minimize the fuel expenditure. The specific demonstrations in the Earth–Moon circular restricted three–body problem found a favorable performance of the regularized method with respect to convergence results and computational speed in comparison with that of the non–regularized one adopting the mass–leak technique.

Declaration of Competing Interest

The author declares that he has no known competing financial interests or personal relationships that could have appeared to influence the work reported in this paper.

Acknowledgments

This study has been partially supported by JSPS Grants-in-Aid No.20K14951.

References

Bertrand, R., Epenoy, R., 2002. New smoothing techniques for solving bang–bang optimal control problems: Numerical results and statistical interpretation. Optim. Control Appl. Methods 23, 171–197. https://doi.org/10.1002/oca.709.

Betts, J.T., 1998. Survey of numerical methods for trajectory optimization. J. Guid. Control Dyn. 21, 193–207. https://doi.org/10.2514/2.4231.

Bokelmann, K.A., Russell, R.P., 2020. Optimization of impulsive Europa capture trajectories using primer vector theory. J. Astronaut. Sci. 67, 485–510. https://doi.org/10.1007/s40295-018-00146-z.

Broucke, R., 1971. Periodic collision orbits in the elliptic restricted three–body problem. Celest. Mech. 3, 461–477. https://doi.org/10.1007/BF01227792.

Celletti, A., 2006. Basics of regularization theory. In: Steves, B.A., Maciejewski, A.J., Hendry, M. (Eds.), Chaotic Worlds: From Order to Disorder in Gravitational N-Body Dynamical Systems vol. 227, pp. 203–230. https://doi.org/10.1007/978-1-4020-4706-0_7.

Conway, B., 2010. Spacecraft Trajectory Optimization. Cambridge University Press, Cambridge.

Doedel, E.J., Paffenroth, R.C., Keller, H.B., Dichmann, D.J., Galán-Vioque, J., Vanderbauwhede, A., 2003. Computation of periodic solutions of conservative systems with application to the 3–body problem. Int. J. Bifurc. Chaos 13, 1353–1381. https://doi.org/10.1142/S0218127403007291.

Ellison, D.H., Englander, J.A., Ozimek, M.T., Conway, B.A., 2014. Analytical partial derivative calculation of the sims-flanagan transcription match point constraints. In: 24th AAS/AIAA Space Flight Mechanics Meeting, AAS 14–310, Santa Fe, New Mexico, Jan. 2014.

Gill, P.E., Murray, W., Wright, M.H., 1981. Practical Optimization. Academic Press, London.

Hénon, M., 1969. Numerical exploration of the restricted problem. V. Hill's case: periodic orbits and their stability. A&A 1, 223–238.

Hénon, M., 1974. Vertical stability of periodic orbits in the restricted problem II. Hill's case. A&A 30, 317–321.

Jiang, F., Baoyin, H., Li, J., 2012. Practical techniques for low–thrust trajectory optimization with homotopic approach. J. Guid. Control. Dyn. 35, 245–258. https://doi.org/10.2514/1.52476.

Koon, W.S., Lo, M.W., Marsden, J.E., Ross, S.D., 2011. Dynamical Systems, the Three-Body Problem and Space Mission Design. Marsden Books, Wellington.

Lam, T., Whiffen, G.J., 2005. Exploration of distant retrograde orbits around Europa. In: 15th AAS/AIAA Space Flight Mechanics Meeting, AAS 05–110, Copper Mountain, Colorado, Jan. 2005.

Mazouffre, S., 2016. Electric propulsion for satellites and spacecraft: established technologies and novel approaches. Plasma Sources Sci. Technol. 25, 033002. https://doi.org/10.1088/0963-0252/25/3/033002.

Mingotti, G., Topputo, F., Bernelli-Zazzera, F., 2011. Optimal low–thrust invariant manifold trajectories via attainable sets. J. Guid. Control. Dyn. 34, 1644–1655. https://doi.org/10.2514/1.52493.

Oguri, K., Oshima, K., Campagnola, S., Kakihara, K., Ozaki, N., Baresi, N., Kawakatsu, Y., Funase, R., 2020. EQUULEUS trajectory design. J. Astronaut. Sci. 67, 950–976. https://doi.org/10.1007/s40295-019-00206-y.

Ollé, M., Rodríguez, O., Soler, J., 2020. Analytical and numerical results on families of n–ejection–collision orbits in the RTBP. Commun. Nonlinear Sci. Numer. Simul. 90, 105294. https://doi.org/10.1016/j.cnsns.2020.105294.

Oshima, K., Topputo, F., Campagnola, S., Yanao, T., 2017. Analysis of medium–energy transfers to the Moon. Celest. Mech. Dyn. Astr. 127, 285–300. https://doi.org/10.1007/s10569-016-9727-7.

Oshima, K., 2019. The use of vertical instability of L_1 and L_2 planar Lyapunov orbits for transfers from near rectilinear halo orbits to planar distant retrograde orbits in the Earth-Moon system. Celest. Mech. Dyn. Astr. 131, 14. https://doi.org/10.1007/s10569-019-9892-6.

Oshima, K., 2021. Optimization–aided, low–energy transfers via vertical instability around Earth-Moon L_1. J. Guid. Control. Dyn. 44, 389–398. https://doi.org/10.2514/1.G005159.

Ottesen, D., Russell, R.P., 2021. Unconstrained direct optimization of spacecraft trajectories using many embedded Lambert problems. J. Optim. Theory Appl. 191, 634–674. https://doi.org/10.1007/s10957-021-01884-1.

Ottesen, D., Russell, R.P., 2022. Piecewise Sundman transformation for spacecraft trajectory optimization using many embedded Lambert problems. J. Spacecr. Rockets 59, 1044–1061. https://doi.org/10.2514/1.A35140.

Ozaki, N., Yamamoto, T., Gonzalez-Franquesa, F., Gutierrez-Ramon, R., Pushparaj, N., Chikazawa, T., Dei Tos, D.A., Celik, O., Marmo, N., Kawakatsu, Y., Arai, T., Nishiyama, K., Takashima, T., 2022. Mission design of DESTINY$^+$: Toward active asteroid (3200) Phaethon and multiple small bodies. Acta Astronaut. 196, 42–56. https://doi.org/10.1016/j.actaastro.2022.03.029.

Pan, B., Pan, X., Lu, P., 2019. Finding best solution in low–thrust trajectory optimization by two–phase homotopy. J. Spacecr. Rockets 56, 283–291. https://doi.org/10.2514/1.A34144.

Pritchett, R.E., Zimovan, E.M., Howell, K.C., 2018. Impulsive and low-thrust transfer design between stable and nearly stable periodic orbits in the restricted problem. In: 28th AIAA/AAS Space Flight Mechanics Meeting, AIAA 2018–1690, Kissimmee, Florida, Jan. 2018. https://doi.org/10.2514/6.2018-1690.

Russell, R.P., 2007. Primer vector theory applied to global low–thrust trade studies. J. Guid. Control. Dyn. 30, 460–472. https://doi.org/10.2514/1.22984.

Sidhoum, Y., Oguri, K., 2023. On the performance of different smoothing methods for indirect low-thrust trajectory optimization. In: 33rd AAS/AIAA Space Flight Mechanics Meeting, AAS 23–207, Austin, Texas, Jan. 2023.

Sims, J.A., Flanagan, S.N., 1999. Preliminary design of low–thrust interplanetary missions. In: 1999 AAS/AIAA Astrodynamics Specialist Conference, AAS 99–338, Girdwood, Alaska, Aug. 1999.

Sims, J.A., Finlayson, P.A., Rinderle, E.A., Vavrina, M.A., Kowalkowski, T.D., 2006. Implementation of a low-thrust trajectory optimization algorithm for preliminary design. In: 2006 AIAA/AAS Astrodynamics Specialist Conference, AIAA 2006–6746, Keystone, Colorado, Aug. 2006. https://doi.org/10.2514/6.2006-6746.

Sullivan, C.J., Stuart, J., Anderson, R.L., Bosanac, N., 2021. Designing low–thrust transfers to high–inclination science orbits via hybrid optimization. J. Spacecr. Rockets 58, 1339–1351. https://doi.org/10.2514/1.A34980.

Szebehely, V., 1967. Theory of Orbits: The Restricted Problem of Three Bodies. Academic Press Inc, New York.

Taheri, E., Junkins, J.L., 2018. Generic smoothing for optimal bang–off–bang spacecraft maneuvers. J. Guid. Control. Dyn. 41, 2470–2475. https://doi.org/10.2514/1.G003604.

Topputo, F., 2013. On optimal two–impulse Earth-Moon transfers in a four–body model. Celest. Mech. Dyn. Astr. 117, 279–313. https://doi.org/10.1007/s10569-013-9513-8.

Vallado, D.A., 2013. Fundamentals of Astrodynamics and Applications. Microcosm Press, Hawthorne.

Zhang, C., Topputo, F., Bernelli-Zazzera, F., Zhao, Y., 2015. Low–thrust minimum–fuel optimization in the circular restricted three–body problem. J. Guid. Control. Dyn. 38, 1501–1510. https://doi.org/10.2514/1.G001080.